

Hard X-ray microbeam experiments with a sputtered-sliced Fresnel zone plate and its applications

N. Kamijo,^{a,b*} Y. Suzuki,^b M. Awaji,^b A. Takeuchi,^b H. Takano,^b T. Ninomiya,^c S. Tamura^{b,d} and M. Yasumoto^{e,b}

^aKansai Medical University, Uyama-Higashi 18-89, Hirakata, Osaka 573-1136, Japan, ^bSPring-8, Mikazuki-cho, Hyogo 679-5198, Japan, ^cForensic Science Laboratory of Hyogo Prefecture Police, Koube, Japan, ^dPhotonic Research Institute, AIST (Kansai Center) Ikeda, Osaka, Japan, and ^ePhotonic Research Institute, AIST (Tsukuba Center) Umesono, Tsukuba, Ibaraki, Japan. E-mail: fe2n-kmji@asahi-net.or.jp

Hard X-ray microbeam experiments with sputtered-sliced Fresnel zone plates have been performed. Zone plates with an outermost zone width of 0.25 μm (#FZP1) and 0.1 μm (#FZP2) were fabricated and evaluated. In a scanning X-ray microscopy experiment, a line-and-space pattern with structure as fine as 0.1 μm was resolved using #FZP2 at an X-ray wavelength of 1 \AA . As an application of the microbeam technique, a two-dimensional distribution of constituent elements in forensic samples has been obtained (e.g. section view of human and elephant hairs) using fluorescent scanning microscopy.

Keywords: hard X-ray microbeams; scanning X-ray microscopy; Fresnel zone plates.

1. Introduction

X-ray microscopy, which has been extensively used in soft X-ray domains (so-called water window regions), is now extending to higher photon energies (8–100 keV). This extension will enable new applications like the observation of thicker medical and biological samples in their natural environment, and in material sciences.

With the availability of high-brilliance third-generation synchrotron X-ray sources like SPring-8, interest has increased in developing microfocusing optics which can effectively utilize the high-brilliance and tunable hard X-rays generated from the undulator sources. The X-ray flux density, after being monochromated by an Si(111) double-crystal monochromator, is more than 10^{13} photons $\text{s}^{-1} \text{mm}^{-2}$ at 14.5 keV in a standard undulator beamline at SPring-8. The expected applications are X-ray scanning microscopes (microfluorescence analysis for two-dimensional trace-element mapping, chemical-state imaging and microdiffraction), imaging microscopy and computed microtomography for hard or high-energy X-rays. Submicrometre spatial resolution has already been achieved using the various microfocusing optics now being developed for hard X-rays: grazing-incidence total-reflection mirrors (Takeuchi *et al.*, 2002; Hirai *et al.*, 2000), circular Bragg–Fresnel lenses (Snigirev *et al.*, 1995), compound refractive lenses (Lengeler *et al.*, 2001; Kohmura *et al.*, 2001) and two types of Fresnel zone plates (FZPs), one fabricated by lithography-based techniques (applicable energy range is below 10 keV at present) (Yun *et al.*, 1999; Di Fabrizio *et al.*, 1999; Suzuki, Takeuchi *et al.*, 2001; Kagoshima *et al.*, 1999) and the other by sputtered-sliced techniques (energy range is greater than 8 keV) (Suzuki, Awaji *et al.*, 2001; Kamijo *et al.*, 1997, 2001). A spatial resolution of $\sim 0.8 \mu\text{m}$ has been achieved for 8 keV X-rays with a grazing-incidence mirror in the Kirkpatrick–Baez configuration, 0.7 μm has been obtained with

the circular Bragg–Fresnel lens for 7.6 keV X-rays, and 0.1–0.3 μm with lithography FZPs for 8 keV X-rays. The lithography FZP, which provides the highest spatial resolution for low-energy X-rays (less than ~ 4 keV), is usually limited in its aspect ratio (height/width of the finest zone) to around unity, though a thicker one usable at 4–10 keV has been recently fabricated (Suzuki, Takeuchi *et al.*, 2001; Kagoshima *et al.*, 1999). To overcome the aspect ratio limitation inherent in the usual lithography technique, the sputtered-sliced FZP (ss-FZP) method has been applied. In this technique, two different materials of heavy and light elements are alternately deposited on a rotating fine gold wire core to give a concentric multilayer structure. The ss-FZP is then produced from the multilayer wire sample by slicing it perpendicular to the wire axis and then thinning and polishing the slice down to the required thickness (10–50 μm). Here, the central gold wire acts as a central stop of the FZP. While a thick FZP for focusing high-energy X-rays can be easily fabricated by this technique, it is not easy to make a thin zone plate for low-energy X-rays due to the grinding/polishing process involved.

Over the last decade we have fabricated ss-FZPs and performed focusing experiments at various X-ray energies. A spatial resolution of 0.5–0.7 μm has been achieved for X-ray energies of 8–29 keV (Suzuki, Awaji *et al.*, 2001). Further, a focused beam of much higher energy (83 keV) has recently been obtained using the ss-FZP (Kamijo *et al.*, 1999).

Here, the recent development of the fabrication technique, the test of resistance to the high-flux X-ray beam (heat load and radiation damage test) and the focusing evaluation of the ss-FZPs at SPring-8 are described. Preliminary results of a scanning X-ray microscopy experiment with the FZP are also given.

2. Zone plate fabrication

Fig. 1 shows the process sequence of the ss-FZP fabrication. Alternate multilayer zones were deposited by d.c.-magnetron sputtering. There are two d.c.-sputtering targets positioned 90° apart with respect to the wire target. The diameter of each sputter target is 102 mm and the target-to-wire distance is 50 mm. The Al (transparent) and Cu (opaque) concentric multilayers (total 40–100 layers) were deposited onto a rotating fine Au wire core (radius 25 μm) at a rotation speed of 15 r.p.m. (Tamura *et al.*, 1997). The radii of the zone boundaries in a ss-FZP are given to a high degree of accuracy by

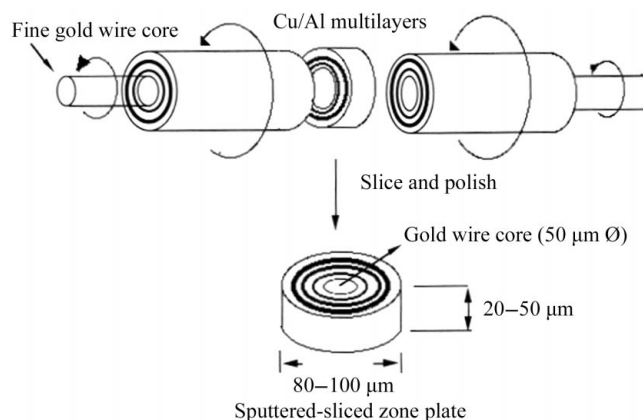


Figure 1
Outline view of the fabrication process for a sputtered-sliced Fresnel zone plate.

Table 1
Zone plate parameters (Cu/Al system).

	#FZP1	#FZP2
Outermost zone width	0.25 μm	0.1 μm
Central stop diameter (gold wire core diameter)	50 μm	50 μm
Primary focal length at 12.4 keV ($\lambda = 1 \text{ \AA}$)	220 mm	68 mm
Number of zones	50	50
Zone plate diameter	80 μm	70 μm
Thickness of zone plate	$\sim 20 \mu\text{m}$	$\sim 29 \mu\text{m}$

$$r_n = (r_0^2 + n\lambda f)^{1/2} \quad (1)$$

for hard X-rays, where r_n is the radial distance of the n th boundary, r_0 is the wire core radius, λ is the wavelength and f is the focal length.

Two kinds of FZPs were prepared. Fig. 2 shows the SEM micrographs of these FZPs. The parameters are given in Table 1. The outermost zone width was 0.25 μm for #FZP1 and 0.1 μm for #FZP2. During deposition, the film thickness was measured using a quartz thickness monitor. As described in previous papers, interface roughness of the outer concentric layers was observed in all fabricated ss-FZPs which may depend upon the sputtering conditions (Saitoh *et al.*, 1988). Ar gas pressure is one case. Lower Ar gas pressure was found to result in smoother zone boundaries. Then the sputtering powers obtained were 6 W cm^{-2} for Cu and 10 W cm^{-2} for Al, and Ar gas pressure was 0.2 Pa (Tamura *et al.*, 1997). Another factor may be the oblique incidence of the sputtering atoms onto the substrate. This may cause shadowing at the surface of the thin film (Thornton, 1986). In order to reduce the oblique components of the beam, a cylindrical slit (diameter 40 mm, length 60 mm, slit width 7 mm, and facing the sputtering target) was installed between the target and the wire substrate (Yasumoto *et al.*, 2001). The deposition rate was 0.3 nm s^{-1} during the growth of the multilayer film with the slit and 1.5 nm s^{-1} without the slit. The FZP (#FZP2) was fabricated by installing the slit, whereas #FZP1 was fabricated without one. The roughness of the outer zone boundaries for #FZP2 was improved compared with those of #FZP1.

After deposition the wire sample was fixed into melted solder, tightened, and sliced into a plate normal to the wire axis (size $\sim 12 \text{ mm} \times \sim 12 \text{ mm} \times \sim 1 \text{ mm}$) using a microcutting machine (band saw impregnated with diamond powder). Then the sample was fixed onto a graphite plate (thickness $\sim 1 \text{ mm}$; Panasonic graphite,

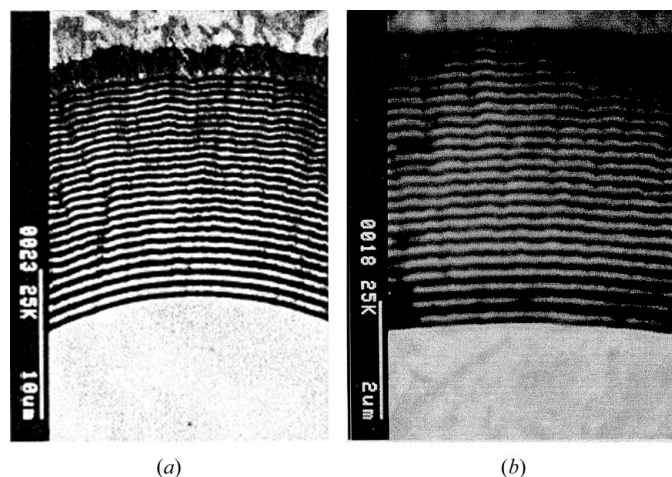


Figure 2
SEM micrographs showing cross sections of Cu/Al concentric multilayers on Au wire core. Fresnel zone plate with an outermost zone widths of (a) 0.25 μm and (b) 0.1 μm .

Matsushita Electronic Industrial Co.), and was polished by a micro-grinding machine using sand paper or a suspension of 2 μm Al_2O_3 powder. After polishing one side, the sample was turned over, fixed again on the graphite plate by Loctite 420 (Nihon Loctite Co.), and the other side was polished. The thickness of the FZP could then be adjusted to be 10–50 μm . The zone plate fabricated in this manner has been tested at various X-ray energies, 8–30 keV (Suzuki, Awaji *et al.*, 2001).

For a typical FZP (amplitude-modulating zone plate), focus is due to the constructive interference of X-rays from each transparent zone. X-rays that would destructively interfere are blocked by the opaque zones. As the zone plate is made thinner, the opaque zones start to transmit some X-rays. Each Cu layer not only absorbs some X-rays but also causes a phase shift of the incident photon. When the relative phase shift between adjacent zones becomes an odd integral multiple of half a wavelength (π), adjacent zones start to constructively interfere. The focusing efficiency of this phase-modulating zone plate (PFZP) with square zone profile can be expressed as

$$\eta_m = [1 + \exp(-2kt\beta) - 2 \exp(-kt\beta) \cos kt\delta] / m^2 \pi^2, \quad (2)$$

where $m = \pm 1, \pm 3, \pm 5, \dots$ and $k = 2\pi/\lambda$, t is the zone plate thickness, and $n = 1 - \delta - i\beta$ is its refractive index. η_m is zero for the even orders. In the ideal case ($\beta = 0$) the focusing efficiency of a phase zone plate reaches 40% for the first-order focus, which is four times higher than that of an amplitude zone plate (large $t\beta$ case) (Kirz, 1974). Calculation of the diffraction efficiencies was performed for our Cu/Al zone plate at various photon energies and at various thicknesses (Kamijo *et al.*, 1999). Thicknesses of 20 μm and 29 μm were obtained for #FZP1 and #FZP2, respectively. The former was appropriate for a phase zone plate at 12.4 keV, the diffraction efficiency being $\sim 17\%$. The latter was thicker, the efficiency being below $\sim 15\%$. Here, an estimate of the zone plate thickness was made by measuring the X-ray transmission rate at the solder area fixing the FZP.

3. Characterization of the zone plate

3.1. Test of resistance of the ss-FZP to the high-flux X-ray beam

The experiment was performed at beamline 47XU of SPring-8, an undulator beamline with an Si(111) double-crystal monochromator. The monochromator crystals are cooled by liquid nitrogen. Both the first and the second crystals are kept at the same temperature to achieve a constant exit beam position. The tunable energy range is 6–37 keV. The distance between the source point and the experimental station is 50 m, and the source size is $\sim 40 \mu\text{m}$ (vertical) \times 800 μm (horizontal).

By directing a full power X-ray beam ($\sim 10^{14}$ photons $\text{s}^{-1} \text{ mm}^{-2}$) at 14.4 keV and ring current 70 mA onto the surface of the ss-FZP, its temperature was measured using a radiation thermometer (calibrated using a thermocouple) which gave readings between 300 and 307 K. The ss-FZP was, thus, proven to be safe with respect to heat load. However, the resin glue ‘LOCTITE 420’ fixing the FZP onto the graphite plate was chemically damaged during full power X-ray irradiation (longer than 20 min exposure). Small bubbles appeared in the solder film embedding the FZP, and a part of the film showed swelling. After that the ss-FZP was broken away. To prevent this serious damage we tried irradiating the surface of the FZP with the full power X-ray beam for 8 h before thinning finally. If this was carried out when the thickness of the FZP was greater than 150 μm , no bubbles or swelling was found. After pre-illumination by X-rays we tried to thin carefully to the desired thickness. The FZP (pre-

illuminated) could work permanently under full-power X-ray irradiation.

3.2. Measurement of the focused beam profiles with #FZP1 by knife-edge scanning

The experiment was performed at hutch #2 of beamline 20XU of SPring-8, a new undulator beamline with an Si(111) double-crystal monochromator for hard X-ray microscopy and medical imaging. The distance between the undulator light source and the experimental station (hutch #2) was ~ 250 m and the source size was ~ 50 μm (vertical) \times 800 μm (horizontal). The monochromator was placed at 46 m from the source point. A liquid-nitrogen cooling system is employed for the monochromator. A slit was installed in the beamline, 200 m upstream of the FZP, for creating a stable pseudo light source. Here, a horizontal slit (50 μm in width) was installed. Therefore, the horizontal focus is a demagnified image of the slit, whereas the vertical focus is generated by demagnification of the undulator source. The distance between the pseudo light source and the FZP was 200 m. The X-ray energy was chosen to be 12.4 keV. An OSA (order-sorting aperture, made from a tantalum plate, 20 μm in diameter and 0.2 mm in thickness) was placed between the FZP and the focal point to select the first diffracted order. An ion chamber or scintillation counter was used in the intensity measurements.

The designed outermost zone width of #FZP1 used here was 0.25 μm . Thus the diffraction limit of the first-order focus of the FZP, $1.2d_n$ (where d_n is the outermost zone width), is 0.3 μm . Knife-edge scanning was performed using a gold wire (200 μm in diameter) as the 'knife-edge' in transmission geometry. The measured intensity profiles were differentiated to obtain the focused beam shape. The minimum focusing size obtained was 0.3 μm full width at half-maximum (FWHM) for the horizontal direction as shown in Fig. 3, and the focal length obtained was 220 mm.

The geometrical magnification factor (M) in the beamline is defined by $M = f/L$, where f is the focal length of the FZP and L is the distance between the pseudo light source and the FZP (200 m). Thus, the focused beam size determined by the geometrical optics, 0.06 μm , is smaller than the diffraction-limited resolution of #FZP1 and, therefore, the FZP was coherently illuminated. The focal spot size obtained here (0.3 μm) agrees well with the theoretical limit of the FZP with outermost zone width of 0.25 μm .

Diffraction efficiency for the first-order light was estimated by comparing the incident beam intensity through the OSA and the total intensity of the focused beam through the OSA. The observed efficiency, $\sim 15\%$, agrees well with that of the calculated one at 12.4 keV.

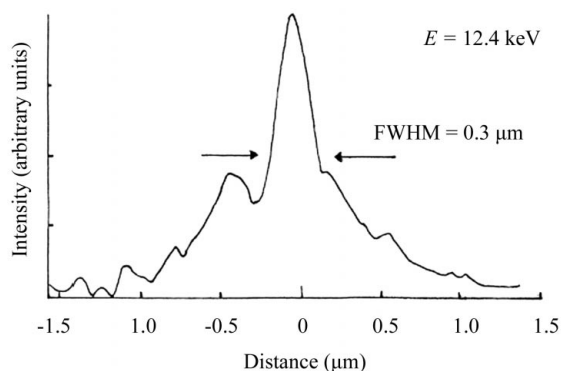


Figure 3 Focused beam profile measured by a knife-edge horizontal scan at 12.4 keV. The full-line curve is the numerical derivative of the raw intensity data.

3.3. Resolution measurement of #FZP2 using scanning microscopy with a test pattern

The scanning microscopy experiment was performed at hutch #1 of beamline 20XU for the resolution measurement of #FZP2. The distance between the undulator light source and the experimental station (hutch #1) was ~ 78 m. A slit was installed in the beamline, 30 m upstream of the FZP, for creating a stable pseudo light source. Here, a horizontal slit (10 μm in width) was installed, and the FZP was also coherently illuminated. A schematic view of the experimental set-up is shown in Fig. 4, which is similar to that of hutch #2 except for the geometrical distances between the undulator source (or pseudo light source) and various optical elements in the beamline.

The designed outermost zone width of #FZP2 used here is 0.1 μm . Thus the diffraction limit of the first-order focus of the FZP is 0.12 μm .

The observation of a scanning microscopic image of the test pattern with fine structures is a method which may be used for measuring the focal beam size (Suzuki, Awaji *et al.*, 2001). We performed a scanning microscopy experiment with a test pattern made of a tantalum microstructure deposited on an Si_3N_4 membrane. It has fine patterns made of 0.5 μm -thick tantalum and having a finest structure of 0.1 μm line-and-space. A schematic view of a fine portion of the test pattern is shown in Fig. 5(b) (Suzuki, Awaji *et al.*, 2001).

The result of a scanning microscopy experiment at an X-ray energy of 12.4 keV is shown in Fig. 5(a). Here, the transmission image was obtained using an ion chamber. The fine pattern down to 0.1 μm has been resolved in the measured image. Therefore, the limiting resolution of the microscope is estimated to be better than 0.2 μm , which is close to the diffraction-limited resolution of #FZP2. The total flux of the microbeam obtained is $\sim 10^9$ photons s^{-1} .

4. Example of a scanning microscope image

A hard X-ray scanning microscope opens the possibility of combining X-ray imaging and chemical species analysis. As a preliminary example we have performed trace-element mapping with fluorescent X-rays using the microprobe obtained here. The experiment was performed at beamline 47XU using the FZP (#FZP1). A horizontal slit (10 μm in width) was installed in the beamline, upstream of the FZP, for the purpose of creating a pseudo source. The distance between the pseudo light source and the FZP is 9 m. The scanning microscopy was performed by raster-scanning the sample with the same translation stage used in knife-edge scanning. The experimental set-up was similar to that of Fig. 4. The X-ray energy for the microbeam was selected to be 12.4 keV ($\lambda = 1 \text{ \AA}$). Two kinds of forensic samples (section view of human and elephant hairs) were prepared. The samples were sliced into ~ 50 μm sections by using a freeze-drying method. Many trace elements were included in both samples (Ninomiya, 2000). Here, mapping of the Zn atom for human hair and of the Fe atom for elephant hair was performed. Zn K_α and Fe K_α fluorescent X-rays were measured using a Ge solid-state detector. In Fig. 6 a section view of the Zn atom (Zn K_α) in human hair is shown. It shows that there is some concentration in Zn atom distribution in the sample.

In Fig. 7 a section view of the Fe atom (Fe K_α) in elephant hair is shown. It shows a very characteristic picture, Fe atoms being concentrated only in the peripheral region of the sample. This might be of interest for studying the metabolism of the elephants which depends on their living environment. We have not performed experiments for other heavy elements included in both samples. These experiment will be performed in the future.

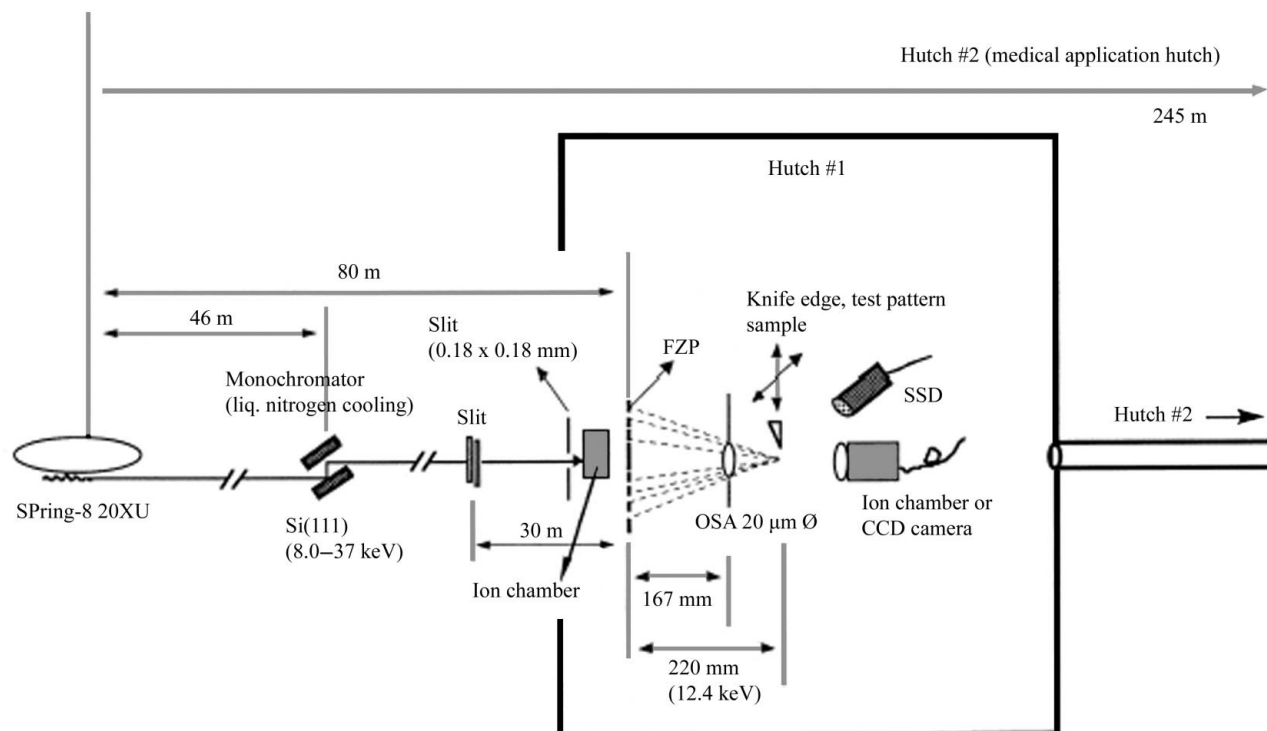


Figure 4
Schematic optical view of Fresnel zone plate evaluation and scanning X-ray microscopy.

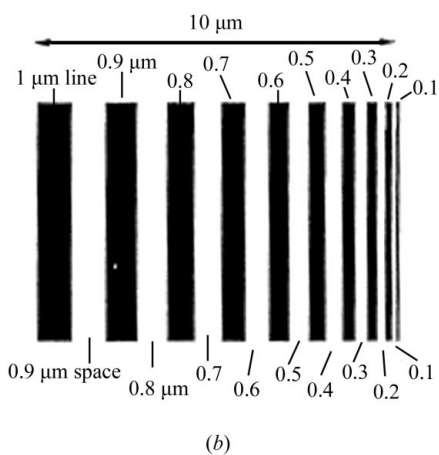
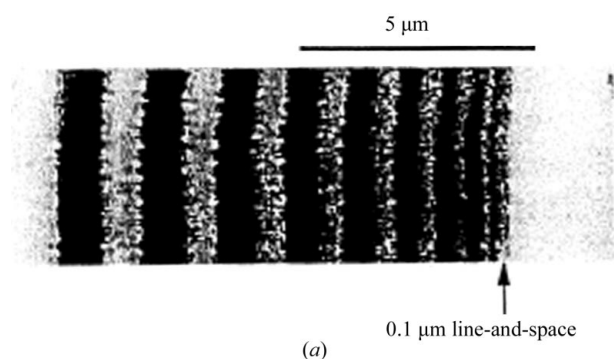


Figure 5
Scanning microscopy image of resolution test pattern. (a) Measured image: X-ray wavelength = 1 Å, 256×70 pixels, $0.0625 \mu\text{m pixel}^{-1}$, dwell time = 0.4 s pixel^{-1} . (b) Schematic diagram of the test pattern at the central area of the measured image.

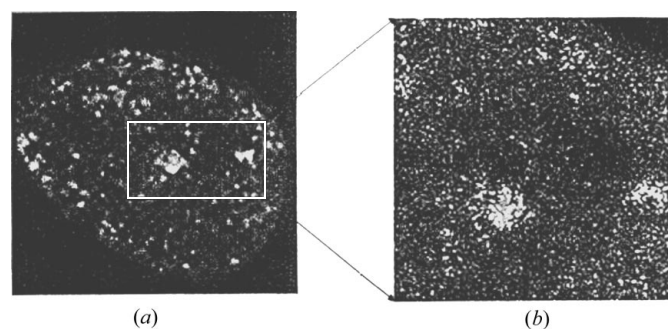


Figure 6
 $\text{Zn } K_{\alpha}$ fluorescence X-ray image of a human hair sample. (a) Whole section view: $2 \mu\text{m pixel}^{-1}$, 64×64 pixels, 0.5 s pixel^{-1} . (b) Close-up view: $0.5 \mu\text{m pixel}^{-1}$, 128×128 pixels, 0.4 s pixel^{-1} .

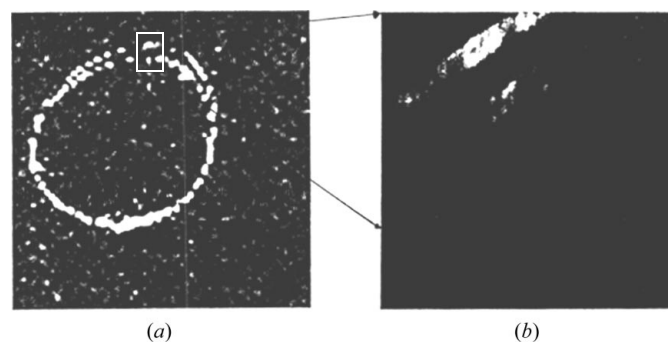


Figure 7
 $\text{Fe } K_{\alpha}$ fluorescence X-ray image of an elephant hair sample. (a) Whole section view: $15.6 \mu\text{m pixel}^{-1}$, 64×64 pixels, 0.5 s pixel^{-1} . (b) Close-up view: $0.5 \mu\text{m pixel}^{-1}$, 256×256 pixels, 0.2 s pixel^{-1} .

5. Conclusions

We have developed sputtered-sliced Fresnel zone plates for hard X-ray focusing. They are genuine X-ray optical elements like those in the soft X-ray domain, though the numerical aperture is quite small (of the order of 10^{-4}). The measured spatial resolution was 0.1–0.3 μm at X-ray wavelengths in the range 0.45–1.5 \AA . The energy of application, 8–100 keV, is possible by changing the thickness of the FZP. A flux density of 10^9 photons $\text{s}^{-1} \mu\text{m}^{-2}$ was obtained in the hard X-ray domain.

The synchrotron radiation experiments were performed at SPring-8 with approval of Japan Synchrotron Radiation Institute (proposal No. 2000B0168-NM-np).

References

- Di Fabrizio, E., Romanato, F. & Gentili, M. (1999). *X-ray Microscopy: Proceedings of the Sixth International Conference*, pp. 635–640. New York: American Institute of Physics.
- Hirai, Y., Hasegawa, M. & Hisada, A. (2000). *SPring-8 User Experiment Report*, No. 5, p. 363. SPring-8, Hyogo, Japan.
- Kagoshima, Y., Takai, K., Ibuki, T., Yokoyama, K., Takeda, S., Urakawa, M., Tsusaka, Y. & Matsui, J. (1999). *X-ray Microscopy: Proceedings of the Sixth International Conference*, pp. 668–671. New York: American Institute of Physics.
- Kamijo, N., Suzuki, Y., Awaji, M., Takeuchi, A., Uesugi, K., Yasumoto, M., Tamura, S., Kohmura, K., Duevel, A., Rudolph, D. & Schmahl, G. (2001). *Nucl. Instrum. Methods*, **A467/468**, 868–871.
- Kamijo, N., Suzuki, Y., Tamura, S., Awaji, M., Yasumoto, M., Kohmura, Y., Handa, K. & Takeuchi, A. (1999). *X-ray Microscopy: Proceedings of the Sixth International Conference*, pp. 672–675. New York: American Institute of Physics.
- Kamijo, N., Tamura, S., Suzuki, Y., Handa, K., Takeuchi, A., Yamamoto, S., Ando, M., Ohsumi, K. & Kihara, H. (1997). *Rev. Sci. Instrum.* **68**, 14–16.
- Kirz, J. (1974). *J. Opt. Soc. Am.* **64**, 301–309.
- Kohmura, Y., Okada, K., Takeuchi, A., Takano, H., Suzuki, Y., Ishikawa, T., Ohigashi, T. & Yokosuka, H. (2001). *Nucl. Instrum. Methods*, **A467/468**, 881–883.
- Lengeler, B., Schroer, C. G., Benner, B., Guenzler, T. F., Kuhlmann, M., Tuemmler, J., Simonovici, A. M., Drakopoulos, M., Snigirev, A. & Snigireva, I. (2001). *Nucl. Instrum. Methods*, **A467/468**, 944–950.
- Ninomiya, T. (2000). Private communications.
- Saitoh, K., Inagawa, K., Kohra, K., Hayashi, C., Iida, A. & Kato, N. (1988). *Jpn. J. Appl. Phys.* **27**, L2131–L2133.
- Snigirev, A., Snigireva, I., Engstroem, P., Lequien, S., Suvorov, A., Hartman, Ya., Chevallier, P., Idir, M., Legrand, F., Soullie, G. & Engrand, S. (1995). *Rev. Sci. Instrum.* **66**, 1461–1463.
- Suzuki, Y., Awaji, M., Kohmura, Y., Takeuchi, A., Takano, H., Kamijo, N., Tamura, S., Yasumoto, M. & Handa, K. (2001). *Nucl. Instrum. Methods*, **A467/468**, 951–953.
- Suzuki, Y., Takeuchi, A., Takano, H., Ohigashi, T. & Takenaka, H. (2001). *Jpn. J. Appl. Phys.* **40**, 1508–1510.
- Takeuchi, A., Suzuki, Y. & Takano, H. (2000). To be published.
- Tamura, S., Mori, K., Maruhashi, T., Yoshida, K., Ohtani, K., Kamijo, N., Suzuki, Y. & Kihara, H. (1997). *Mater. Res. Soc. Symp. Proc.* **441**, 779–784.
- Tamura, S., Yasumoto, M., Mihara, T., Kamijo, N., Suzuki, Y., Awaji, M., Takeuchi, A., Takano, H. & Handa, K. (2001). *Proceedings of the Sixth International Symposium on Sputtering and Plasma Process (ISSP 2001)*, pp. 353–356. ISSP 2001 Committee.
- Thornton, J. A. (1986). *J. Vac. Sci. Technol.* **A4**, 3059–3065.
- Yasumoto, M., Tamura, S., Kamijo, N., Suzuki, Y., Awaji, M., Takeuchi, A., Takano, H., Kohmura, Y. & Handa, K. (2001). *Jpn. J. Appl. Phys.* **40**, 4747–4748.
- Yun, W., Lai, B., Cai, Z., Maser, J., Legnini, D., Gluskin, E., Chen, Z., Kranoperova, A. A., Vladimirov, Y., Cerrina, F., Di Fabrizio, E. & Gentili, M. (1999). *Rev. Sci. Instrum.* **70**, 2238–2241.